AN ELECTROSTATIC INDUCTION MICROMOTOR SUPPORTED ON GAS-LUBRICATED BEARINGS

Luc G. Fréchette[2*], Steven F. Nagle[1], Reza Ghodssi[3], Stephen D. Umans[1], Martin A. Schmidt[1], Jeffrey H. Lang[1]

[1]Dept. of Electrical Engineering and Computer Science,
Massachusetts Institute of Technology, Cambridge, MA 02139

[2]Dept. of Mechanical Engineering, Columbia University, New York, NY 10027

[3]Dept. of Electrical and Computer Engineering, University of Maryland, College Park, MD 20740

ABSTRACT

This paper reports the first successful fabrication and demonstration of an electrostatic induction micromotor supported on gas-lubricated bearings for electrical-to-mechanical energy conversion. The device consists of a stack of five (5) deep reactive ion etched (DRIE) fusion bonded silicon wafers, with an enclosed 4.2 mm diameter rotor driven by a high-voltage, high-frequency thin-film stator. Testing has demonstrated a torque of 0.3 μNm at a rotation rate of 15,000 revolutions per minute, corresponding to a shaft power of 0.5 mW. This development effort serves to support the creation of a wide array of power MEMS devices such as micro-scale pumps, compressors, generators, and coolers [1].

INTRODUCTION

Rotating machines, such as motors and generators, are commonly used for actuation purposes (moving mechanisms) and energy conversion. Through microfabrication approaches such as polysilicon surface micromachining and high-aspect ratio LIGA processing, MEMS electrostatic and magnetic micromotors [2,3] have brought some of these functionalities to the micro-scale. By design, typical power levels of current micromotors range from picowatts to milliwatts, making them mostly suitable as drives for micro-actuators. If designed for high speed and high torque, microfabricated motors could also provide electrical-to-mechanical energy conversion on the order of watts. The envisioned applications for such micromachines include dime-sized gas-turbine generators powering mobile electronic devices, motor-driven pumps and compressors for handheld analytical instruments, or micro-coolers for electronics, sensors, or people [1]. An on-going effort at MIT has demonstrated other power MEMS components such as microfabricated combustors (chemical-to-fluid energy conversion) [4], micro-turbomachinery (fluid-to-mechanical energy conversion) [5], high-speed gas bearings [5], as well as the enabling silicon fabrication technologies [6,7].

The current device is aimed at the development and characterization of an electrostatic induction micromotor supported on high-speed gas-lubricated bearings for electrical-to-mechanical energy conversion. This paper will describe the device design and operation, summarize the fabrication approach and challenges encountered, and describe the micromotor characterization and initial test results.

DEVICE DESIGN AND DESCRIPTION

The device, illustrated in Figure 1, consists of a 4.2 mm diameter and 300 μm thick single crystal silicon rotor enclosed in a fusion-bonded stack of five wafers. The rotor is driven by a planar electrostatic induction micromotor located on the aft side of the disk, and is allowed to rotate freely by suspending it on gas-lubricated bearings. In this characterization device, the load on the rotor consists of the viscous drag in the motor gap and in the bearings. The forward side of the rotor (facing wafer #2) is intended as the location of a radial compressor for a micro-compression system [8].

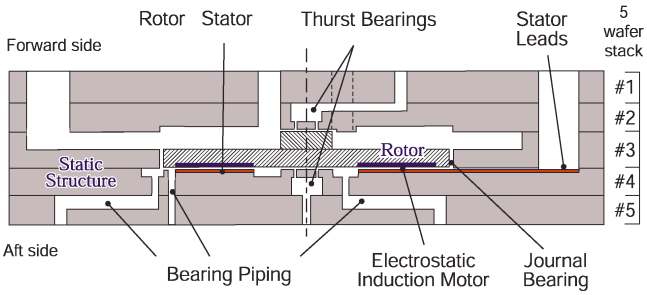

***Figure 1** - Schematic cross-section of the induction micromotor integrated with pressurized gas bearings in a 5-wafer bonded stack.*

Gas-lubricated bearings - A pair of hydrostatic thrust bearings floats the rotor in the axial direction, while a hydrostatic journal bearing on the periphery of the rotor provides a gas film for lateral support. The bearings are fed with externally pressurized gases, which flow through micron scale clearances to apply controlled hydrostatic pressure forces on the rotor. As shown in Figure 1, deep reactive ion etched (DRIE) channels and holes in the bonded wafers create the fluidic piping to pressurize the gas bearings. The bearings are designed such that a disturbance of the rotor position will create an asymmetric pressure field on the rotor, which results in a restoring net force. The development and successful operation of this hydrostatic bearing system up to 1.4 million revolutions per minute has been reported previously [5,6], so the focus of this paper is on the micromotor and its integration in the 5-wafer stack.

Electrostatic induction micromotor - The motor consists of a poorly conducting film on the backside of the rotor disk, separated by an air gap from a polar array of 786 radial electrodes forming the stator surface [9]. By applying a circumferentially traveling potential waveform on the stator surface, charges are induced in the rotor film and dragged along with the stator potential wave.

* Corresponding author: lucf@alum.mit.edu - Phone: (212) 854-2962

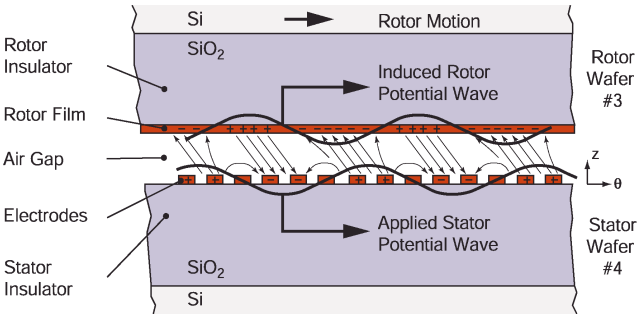

***Figure 2** - Induction micromotor operating principle, illustrating the electrostatic torque applied by the tangential component of the electric fields.*

For a finite conductivity of the rotor film, the induced rotor potential wave and charges tend to lag behind the stator potential wave, as illustrated in Figure 2, such that the tangential component of the electrical field lines produce a torque on the rotor[1]. The relative velocity of the rotor with respect to the applied stator potential wave is a main operating parameter, defined as the slip $S = (\omega - m\,\Omega) / \omega$, where ω is the electrical frequency, Ω is the rotor speed, and m is the number of pole pairs. As the slip is increased, the motor torque will initially increase, reach a maximum value (peak torque), and then gradually decrease. The rotor film resistivity sets the value of slip at which the peak torque is achieved. Based on analytical models of the electrostatic forces in induction micromotors [10,11], the configuration presented in Table 1 was designed, as a drive for a micro-compressor [8].

***Table 1** - Induction micromotor design configuration along with the parameters of the fabricated device (shown in parentheses).*

Stator configuration	6 phases / 131 pole pairs	
Motor gap height	3 μm	(4 μm)
Inter-electrode gap	4 μm	(5 μm)
Electrode width	3 to 10 μm	(3 to 10 μm)
Motor radial extend	r_i= 1.0 to r_o=1.9 mm	
Rotor film resistivity	200 MΩ/□	(30 MΩ/□)
Stator rated voltage	±300V	(±100V)

In this implementation, six electrodes (phases) are used to discretize one period (pole pair) of the stator waveform. Each phase is excited with a sinusoid, relatively shifted by 60° from its neighboring phase, to create the traveling potential waveform. For these design parameters, modeling predicts a motor shaft power of 3 watts at a rotation rate of 900,000 revolutions per minute (200 m/s peripheral speed)[2]. The most critical parameters in achieving this level of performance are: small motor gap height g; high voltage V; thick rotor and stator insulation d; and adequate rotor film resistivity (in order to operate at peak torque). This is shown by the following approximate expression for the peak torque [11]:

$$T_{\substack{elec,\\peak}} = \frac{\pi}{4}\,\frac{m\varepsilon_o V^2}{1+\frac{\varepsilon_{SiO_2} g}{\varepsilon_o d}}\,(r_o^2 - r_i^2) \qquad (1)$$

The power requirement drove the design to high frequency (MHz) and voltage (>100V), introducing the need for thick insulation (10 μm SiO_2 layers) to reduce stray capacitance and minimize the field leakage in the rotor substrate.

DEVICE FABRICATION

The fabrication sequence consists of: 1) building the motor components through thin and thick film processing; 2) deep reactive ion etching (DRIE) the flow channels and bearings 3) aligned fusion bonding the five patterned wafers. Overall, the process requires: 25 photolithography steps, 9 deep reactive ion etches, 5 shallow silicon etches, and 14 thin and thick film depositions and etches. It also has four (4) fusion-bonded interfaces, including Si-Si and Si-SiO_2. The DRIE and wafer bonding portions of the sequence (to form the silicon structure) are based on devices built previously and are presented elsewhere [6,5]. The focus in this section is on the motor components and their integration within the silicon structure.

A main process challenge consisted of integrating thick (10 μm) PECVD oxide layers and the electrical components in the bonded wafer stack. An approach similar to that presented by Ghodssi *et al* [7] (with less extensive planarization) was used. The main steps to create the stator shown in Figure 3 consist of first, etching a silicon pit (10 μm deep), then depositing and patterning an 8 μm PECVD SiO_2 film, leaving only islands of oxide in the pits[3]. A two-level interconnect structure, composed of two 1 μm highly phosphorous-doped polysilicon films (interconnect and electrode layers) and a 1 μm TEOS interlevel dielectric, is then built on the recessed oxide islands. The polysilicon layers were removed from the bonding areas, whereas the TEOS film remained. The flow channels are then formed through aligned, double-side, through-wafer deep etching (DRIE).

A similar approach is used for the rotor process flow by first etching 14 μm silicon pits and creating recessed PECVD oxide islands (10 μm thick). LPCVD polysilicon is then deposited, lightly doped, and patterned to form a rotor film (0.5 μm) on the recessed oxide islands. Boron implant conditions were investigated [11], suggesting an implant power of 180 keV and dose of $5x10^{12}$ cm^{-2} in order to achieve the relatively high resistivity (200 MΩ/□) required for a peak torque at 30% slip. The forward side of the wafer is then etched (200 μm DRIE), the rotor wafer is fusion bonded to wafer #2 (previously double-side, aligned, deep etched), and the rotor is formed by etching the journal bearing (300 μm deep by 15 μm wide circular trench).

Finally, wafers #1 and #5 are also deep etched, and the three remaining interfaces are fusion bonded to complete the 5-wafer stack. Successful bonding was found to be very challenging due to the bow induced by stress in the thick films, as well as the surface roughness introduced by multiple thin film depositions. Chemical-Mechanical Polishing (CMP) was used on both sides of the rotor and stator wafers to improve the surface quality (i.e. the initial contact forces). To assemble the current set of 5 wafers, the rotor wafer was subjected to three (3) bonding cycles, each with a 1 hr anneal at 1100ºC and preceded by CMP. As a result of this undesired processing, the electrical properties of the doped polysilicon films are expected to deviate from the design conditions.

[1] The normal component of the electrical fields pulls the rotor towards the stator, which is compensated by increasing the aft thrust bearing pressure.
[2] Such rotational speeds have been achieved using an air turbine to drive the disk [5]

[3] The oxide is only annealed after patterning in order to minimizing the stress-induced wafer bow, since the oxide appears as isolated islands instead of a continuous film.

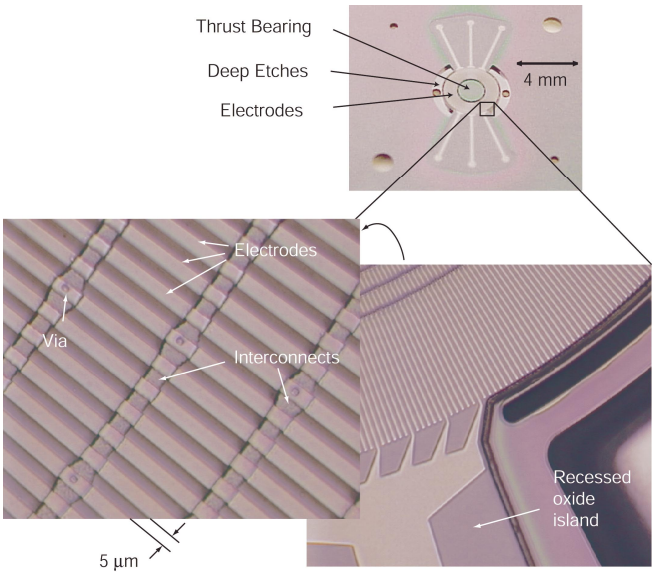

Figure 3 *- Optical picture of the stator surface (wafer #4), showing the DRIE bearing flow paths and the two-level polysilicon electrode structure on 10 μm SiO_2.*

EXPERIMENTAL APPARATUS AND RESULTS

The device requires multiple fluidic and electrical connections, as well as optical access to measure the rotor speed. High-pressure fluidic connections are established by clamping the die between Plexiglas plates with o-rings and machined flow channels. The six motor phases were individually contacted with mechanically aligned spring loaded pogo-pins (IDI). Gold balls were added on the contact pads, using a wire bonder, in order to reduce the contact resistance with the polysilicon stator leads. High-voltage, high-frequency resonant electronics were developed to drive the six phases. Custom inductors and tunable capacitors were connected to each phase, and provided a terminal voltage up to ±300V when excited at 1.8 MHz with digital electronics. The rotor speed was determined from the spectral content of a fiber optic reflectance probe (Philtec Inc.) aimed at the rotor.

An experiment first starts by pressurizing the gas bearings to levitate the rotor, then applying the stator excitation to set the rotor in motion. The rotor reached 15,000 rpm with ±100V, at which point the current and voltage exhibited sudden fluctuations, characteristic of electric field breakdown in the stator. Performance degraded after this apparent breakdown event.

For further characterization of the induction micromotor, individual function generators, synchronized with a pulse generator, were used to drive the six phases of a second device at low voltage. Figures 4 and 5 show the measured rotation rate for the second device as a function excitation frequency and voltage amplitude, respectively. These low voltage results show a behavior characteristic of induction motors, such as a peak torque at a given frequency (~5 MHz for this device) and an approximate quadratic dependency on voltage. Based on the design rotor film resistivity of 200 $M\Omega_{/\square}$, the peak torque was expected at 700 kHz. Based on the models, a peak torque frequency of 5 MHz would imply a resistivity of 30 $M\Omega_{/\square}$ instead. This deviation from the design intent may results from impurities introduced by the CMP and subjected to high temperature cycling during bonding.

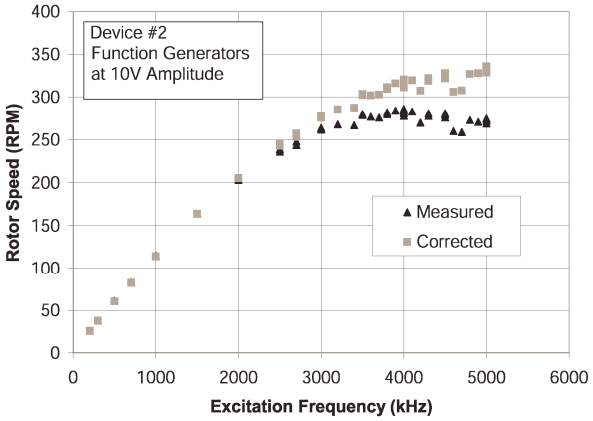

Figure 4 *- Rotation rate as a function of stator excitation frequency, for a sinusoidal ±10V excitation. The corrected data accounts for the gradual drop in source voltage at higher frequency, assuming a quadratic dependence on voltage.*

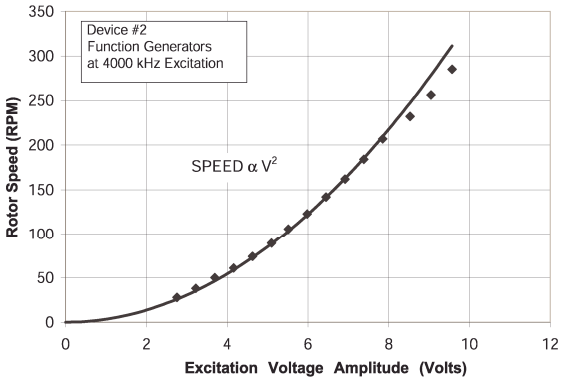

Figure 5 *- Rotation rate as a function of voltage amplitude, at a constant frequency of 4 MHz. The dependence is seen to be approximately quadratic with voltage.*

TORQUE CHARACTERIZATION

The electrostatic motor torque can be derived from the viscous load, using results from a transient spin-down experiment. The experiment consists of suddenly turning off the motor from a steady-state speed Ω_o, and measuring the instantaneous rotational speed as the rotor decelerates due to the opposing viscous load. Based on the Couette flow approximation, the viscous drag is proportional to the rotational speed: $T_{visc} = -K_{visc}\Omega$, suggesting the following deceleration during spin-down:

$$I\frac{d\Omega}{dt} = T_{visc} = -K_{visc}\Omega(t) \;\rightarrow\; \ln\left(\Omega(t) - \Omega_o\right) = -\frac{K_{visc}}{I}t \quad (2)$$

Figure 6 shows the measured instantaneous rotor speed as a function of time on a semi-logarithmic scale for such a spin-down experiment, using the second device. Given the mass moment of inertia of the rotor, I=0.21x10^{-11} kg·m^2, the viscous torque coefficient is found to be K_{visc}= 1.69±0.17 μNm·s. This value is consistent with a calculated value of K_{visc}= 1.72 μNm·s, when assuming simple fully developed Couette flow in all the gaps surrounding the rotor, with nitrogen at ambient temperature.

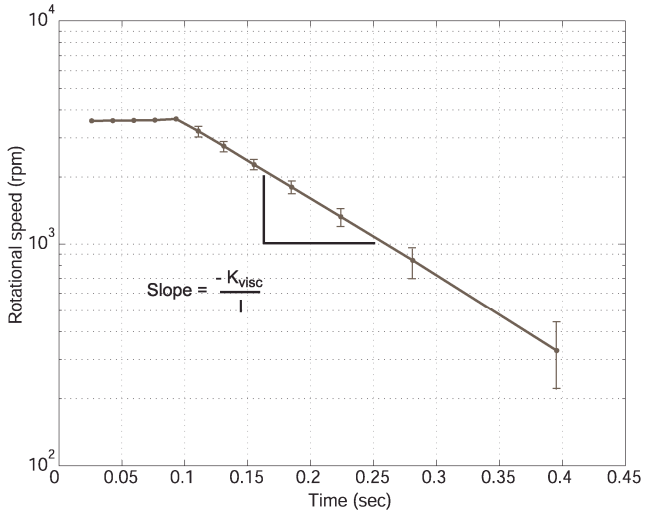

***Figure 6** - Rotational speed as a function of time during the spin-down experiment (Device #2).*

The motor is therefore predicted to deliver a peak torque of 0.3 μNm at 15,000 rpm, with a corresponding shaft power of 0.5 mW. The experimental results from the second device show a torque level of 65 μNm/kV^2 and an approximately quadratic trend with voltage. Based on this torque level, the motor driven at 5 MHz and ±300V could potentially operate up to 300,000 rpm if the trend remains quadratic with voltage. Although our devices exhibited electric field breakdown near 100V, higher voltage operation should be possible since tests on similar electrode structures have withstood up to 300V (as expected from Paschen's curve). The trend with voltage however does not appear to be purely quadratic at higher voltages, as may be seen in Figure 5. Heating of the rotor at high voltages would induce changes in rotor film resistivity and gas viscosity, possibly accounting for the apparent non-quadratic behavior. It should be noted that due to the lower than desired rotor film resistivity, the slip approaches unity and relatively large amounts of power are dissipated in the rotor film, generating heat.

CONCLUSIONS

An electrostatic induction micromotor designed for energy conversion applications was fabricated and integrated with gas-lubricated bearings in a 5-wafer stack. Characterization and testing demonstrated a maximum speed of 15,000 revolutions per minute (3 m/s peripheral speed) achieved under a 1.8 MHz sinusoidal excitation at ±100V. The viscous drag on the rotor was experimentally measured and used to quantify a maximum motor torque of 0.3 μNm and a power of 0.5 mW. The speed was limited by electrical breakdown, occurring in the motor above 100V, and by the limited frequency range of the drive electronics at high voltage. Even below the breakdown threshold, performance seemed to degrade as voltage increased. On-going efforts to increase the performance of the micromotor include the investigation of electric field breakdown conditions and further characterization of the rotor film conductor as a function of temperature and processing conditions.

ACKNOLWEGEMENTS

The authors wish to thank A. H. Epstein, S. D. Senturia, A. A. Ayón, X. Zhang, C. Livermore, and E. P. Warren of MIT for their guidance and hands-on help. The devices were fabricated at the MIT Microsystems Technology Laboratory. This work was supported by DARPA under Dr. R. Nowak (DAAG55-98-1-0365) and also by the Army Research Office under Dr. R. Paur (DAAH04-95-1-0093). Partial support for the first author was also provided by the Fonds pour la Formation de Chercheurs et l'Aide à la Recherche.

REFERENCES

1. A.H. Epstein *et al*., "Micro-Heat Engines, Gas Turbines, and Rocket Engines – The MIT Microengine Project", AIAA Paper 97-1773, *28th AIAA Fluid Dynamics Conference*, Snowmass Village, CO, June 29-July 2, 1997.

2. M. Mehregany, P. Nagakar, S.D. Senturia, and J.H. Lang, "Operation of microfabricated harmonic and ordinary side-drive motors," *Proc. IEEE Workshop on MEMS*, 1-8, Napa Valley, CA February 12-14, 1990.

3. H. Guckel, T. Christenson, K. Skrobis, T. Jung, J. Klein, K. Hartojo, I. Widjaja, "A First Functional Current Excited Planar Rotational Magnetic Micromotor," *Proc. IEEE Micro Electro Mechanical Systems*, Fort Lauderdale, FL, February 1993.

4. A. Mehra, A.A. Ayón, I.A. Waitz, M.A. Schmidt, "Microfabrication of High Temperature Silicon Devices Using Wafer Bonding and Deep Reactive Ion Etching," *J. MEMS*, June 1999.

5. L.G. Fréchette, S.A. Jacobson, F.F. Ehrich, R. Ghodssi, R. Khanna, C.W. Wong, X. Zhang, K.S. Breuer, M.A. Schmidt, and A.H. Epstein, "Demonstration of a Microfabricated High-Speed Turbine Supported on Gas Bearings," *Proc. Solid-State Sensor and Actuator Workshop*, Hilton Head Is. NC, June 2000.

6. C.-C. Lin, R. Ghodssi, A.A. Ayón, D.Z. Chen, S.A. Jacobson, K.S. Breuer, A.H. Epstein, and M.A. Schmidt, "Fabrication and Characterization of a Micro Turbine/Bearing Rig," *Proc. IEEE Micro Electro Mechanical Systems*, Orlando, FL, January 1999.

7. R. Ghodssi, L.G. Fréchette, S.F. Nagle, X. Zhang, A.A. Ayón, S.D. Senturia, and M.A. Schmidt, "Thick Buried Oxide in Silicon (TBOS): An Integrated Fabrication Technology for Multi-Stack Wafer-Bonded MEMS Processes" *Proc. 10th International Conference on Solid-State Sensors*, Sendai, Japan, June 1999.

8. L.G. Fréchette, *Development of a Microfabricated Silicon Motor-Driven Compression System.* Ph.D. Thesis, Massachusetts Institute of Technology, September 2000.

9. S.F. Nagle, J.H. Lang, "A Micro-Scale Electric-Induction Machine for a Micro Gas Turbine Generator" *27th Annual Meeting of the Electrostatics Society of America*, June 1999.

10. S.F. Bart and J.H. Lang, "An analysis of electroquasistatic induction micromotors," *Sensors and Actuators*, **20**, 97-196, November 1989.

11. S.F. Nagle, *Analysis, Design, and Fabrication of an Electric Induction Micromotor for a Micro Gas-Turbine Generator*. Ph.D. Thesis, Massachusetts Institute of Technology, October 2000.